Laser-induced heating and melting of gold nanoparticles studied by time-resolved x-ray scattering

A. Plech* and V. Kotaidis

Fachbereich Physik der Universität Konstanz, Universitätsstrasse. 10, D-78457 Konstanz, Germany

S. Grésillon

ESPCI, 10, rue Vauquelin, F-75005 Paris, France

C. Dahmen and G. von Plessen

I. Physikalisches Institut, RWTH Aachen, D-52056 Aachen, Germany

Pulsed x-ray scattering is used to examine the lattice dynamics in gold nanoparticles in water following excitation with intense femtosecond laser pulses. At lower excitation power the initial lattice heating is followed by cooling on the nanosecond time scale. The decay can be described by solving the heat transfer equations including both the bulk conductivity in water and a finite thermal boundary resistance at the particle-water interface. The lattice expansion rises linearly with excitation power, up to an excitation power corresponding to a lattice temperature increase of 529 K. At higher temperatures the lattice shows a loss of long-range order due to pre-melting of the particles. At the bulk melting temperature, complete melting occurs within the first 100 ps after laser excitation.

I. INTRODUCTION

Dynamical processes in metal nanoparticles currently attract much interest.[1–3] For instance, time-resolved optical experiments have allowed deep insight into electron relaxation processes in noble-metal nanoparticles.[4–7] Another focus of interest is the structural dynamics of nanoparticles, which may significantly differ from the bulk case due to size effects. For instance, if the particle size is in the same range as the mean free path of phonons, the phononic heat transport is changed in comparison to the bulk. Furthermore, the limited size gives rise to shape vibrations, which have been widely studied.[8–16]

Studies of the structural dynamics in metal nanoparticles have mostly been done by time-resolved optical pump-probe spectroscopy (see, e.g., Ref. 4 for a review). In such experiments, the energy absorbed from the pump pulse leads to a heating of the conduction electrons. The probe pulse then samples the changes in the particles' optical properties induced by the pump pulse. These changes are correlated to both the electron heating and the subsequent structural dynamics. Electron-phonon coupling leads to a transfer of the electronic excess energy into lattice heat. Beats in the transient absorption spectra are usually interpreted as shape vibrations of the nanoparticles triggered by the sudden thermal expansion. The period of the oscillations is in most cases identified as that of the lowest-order spherical vibration mode, or breathing mode. Only a few authors report higher-order shape vibrations in time-resolved pump-probe experiments,[17] in contrast to the fact that they are observable in Raman[18,19] or Brillouin scattering.[20]

These oscillations are usually damped within a few cycles of oscillation, due to acoustic coupling to the embedding matrix; decay into thermalized phonons in the nanoparticles

may also contribute to the damping. There seem to be large differences in the damping times, depending on whether particles are embedded into a solid glass matrix (as in the case of silver particles in the works of del Fatti *et al.*[13]) or suspended in water, as in the case of the works of Hartland,[15] where very long damping times are observed.

Subsequent to the thermal equilibration between electrons and lattice, the thermal energy is released to the surrounding environment via phonon-coupling across the particle-matrix interface.[21–24] These cooling times range from a few picoseconds to nanoseconds, depending on environment and size of the particles.[25] Only few investigations address the nature of the heat transfer and the time scales. Hu and Hartland[26] have measured the thermal cooling of gold nanoparticle sols in water and find an almost quadratic dependence of the cooling times on the diameter of the particles. The transient absorption signal is approximately proportional to the particle temperature, and a signal decay close to a stretched exponential as a function of time was reported. This is in agreement with calculations assuming that the bulk heat diffusion in the matrix determines the time scale for cooling. Such behavior has also been found in water oil emulsions.[27] In contrast, in silver-glass systems an exponential decay with a linear dependence of the cooling times on the diameter has been found,[23] representing a limiting case where an interface resistance dominates the transport. Wilson *et al.*[22] give an estimate of the relative importance of both effects and try to determine the nature of the heat transport causing the cooling of Pt nanoparticles.

At high excitation densities, melting of the nanoparticles may occur. Link and El-Sayed[4,28] have investigated the shape transformation of rod-like gold nanoparticles and found time constants of 30 ps for the transition to the stable spherical configuration,[28] a time scale which is comparable to phonon-
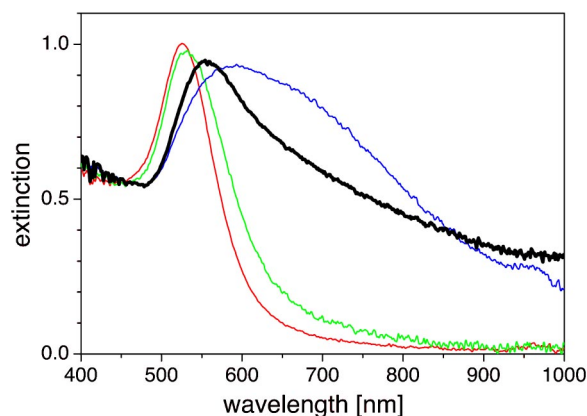
FIG. 1. (Color online) Extinction spectra from samples containing gold nanoparticles with mean diameters of 46, 67, 100, and 133 nm, respectively (plasmon band maximum from left to right). The spectra have been normalized with respect to the atomic gold concentration. The results presented in the following figures have been obtained on the 100 nm particles (thick solid line).

phonon scattering times. Hartland, Hu, and Sader[16] have addressed the problem of the melting transition by searching for discontinuities in the vibrational mode frequency as a function of temperature. The absence of such a discontinuity up to large values of the incident laser power was interpreted as a consequence of bleaching of the interband transitions under intense excitation, which limits the achievable lattice temperature. In bulk semiconductors, high excitation densities may induce a melting transition nonthermally by transferring valence electrons into anti-binding states, which causes the long-range order to vanish within a few picoseconds.[29] A structural phase change during the semiconductor to metal transition in VO_2 was reported to occur within 10 ps after laser excitation.[30]

Here we address the lattice dynamics of optically excited gold nanoparticles in water by time-resolved x-ray scattering. Our method allows us to gain a more direct access to the atomic structure of the particles after laser heating than is possible with purely optical techniques. Lattice expansion and the disappearance of long-range order are direct indications for a melting phase transition. The cooling of the nanoparticles due to heat transfer to the ambient water is analyzed.

II. MATERIALS AND TECHNIQUES

Gold nanoparticles have been synthesized by the well-known citrate method.[31] We control the sizes of the particles by varying the relative concentrations of gold ions with respect to the citrate reductant. In brief, 50 ml of a 0.4 to 1 mM solution of $HAuCl_4$ was brought to boil and 1 ml of hot trisodium citrate solution of typically 0.4–0.8% volume was added quickly. Having a homogeneous boiling temperature at the boiling point was crucial for minimizing the size dispersion.[32] The color of the solution changed from blue to red (and orange for the larger particles as light scattering becomes important) within several minutes (see spectra in Fig. 1). The liquid was kept boiling for 15 min until no

further changes in the optical spectra were observable. Rapidly sedimented parts of the solution were removed and the rest was stable for weeks to be transported to the synchrotron.

Optical extinction spectra (Ocean Optics spectrometer) from different samples produced with this method are shown in Fig. 1. The polaritonic redshift of the plasmon resonance with increasing size is clearly visible. The spectra have been normalized to the same atomic gold concentration. The relation between extinction and absorption at 400 nm has been calculated using Mie theory.[1] We conclude that the absorbed power density at 400 nm does not change strongly with particle size. We therefore believe that particle-size dispersion should not lead to an inhomogeneous excitation of the particle ensemble.

Particle sizes were determined by a scanning electron microscopy (SEM, Hitachi) analysis of particles adsorbed on polyelectrolyte plated silicon substrates.[33,34] The size dispersion is usually around 15%, which is larger than what has been achieved by radiation chemistry techniques.[15] Results of a sample containing gold particles of 100 nm diameter are presented in the following; similar results have been obtained also for other average particle diameters. The x-ray powder scattering performed on the particles reveals that the particles are internally polycrystalline with a mean grain size of 35 nm as derived from the Scherrer formula.[35]

The time-resolved scattering experiments have been performed at the beamline ID09B at the synchrotron radiation source ESRF.[36,37] A femtosecond regenerative Ti:sapphire amplifier system (Spectra Physics, Coherent) has been synchro locked to the radio frequency of the acceleration cavity of the electron storage ring. Thus the emission of laser pulses is synchronous to the time structure of electron pulses within the vacuum ring and therefore also to the emitted x rays at the undulator device. A 235 pole undulator of 17 mm period produces intense x-ray pulses at a center wavelength of 15 keV. They pass through a channel-cut silicon monochromator in order to achieve a relatice energy bandpass of 1.4×10^{-4} at 15 keV.

The pulse repetition frequency of the x-ray emission is about 568 kHz in a time-resolved mode of 16 circulating electron bunches, i.e., much higher than the laser repetition rate of 896 Hz. A matching of the pulse sequence is achieved by a mechanical chopper for the x rays, which runs at the same frequency as the laser and is synchronized to a fixed electron pulse. The delay between laser and x-ray pulses can be varied in steps of 5 ps over a millisecond range. The electronic jitter from the feedback loop of the oscillator cavity (phase lock) determines the actual laser-to-ray timing precision and is much smaller than the x-ray pulselength of 80–110 ps (16 bunch mode). The calibration of coinciding pulses (delay time $\tau=0$) is done by the onset of photo signals as seen in Fig. 2, to a precision better than 20 ps. This setup allows one to apply pump-probe schemes as known from femtosecond optical spectroscopy. A two-dimensional x-ray detector (MarCCD 64 μm pixel size, 133 mm diameter, Mar Research, Hamburg) is used to record the scattering from the crystalline lattice.

The aqueous gold solution is injected into a thin-walled borosilicate capillary (Hilgenberg, Germany) of 0.3 mm di-
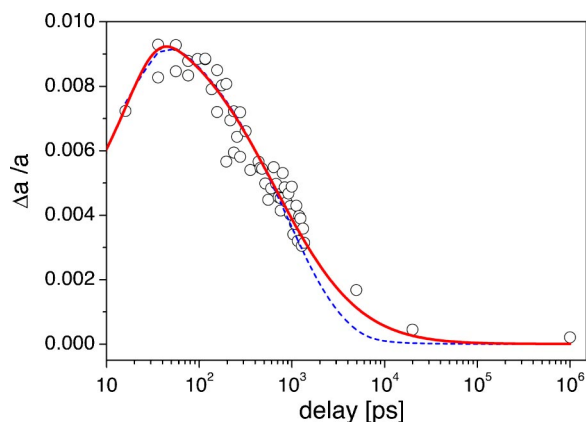
FIG. 2. (Color online) Relative lattice expansion determined from the (111) reflection as a function of the delay time between laser and x-ray pulses. The delay time is plotted on a logarithmic scale to compare the experimental data with the solution of the heat transfer equations (solid line) and a stretched exponential function (dashed line).

ameter. Care is taken to have a sufficient flow to replace the liquid between successive laser shots, using an appropriate flow velocity. Therefore each portion of the sample is only excited once to avoid the accumulation of damage from the laser. The laser and x-ray beams hit the capillary almost collinearly. The laser power is controlled by neutral density filters and calibrated with a laser power meter (Coherent); 150 fs pulses from the regenerative amplifier are frequency doubled to 400 nm and used for sample excitation.

The powder scattering from the nanoparticle solution is integrated azimutally and, after normalization and background subtraction, the peaks are fitted with Lorentz functions. This approach delivers the lattice expansion in the direction of the chosen Bragg planes as well as peak intensities and peak widths as functions of the delay time τ between laser and x-ray pulses. The lattice expansion is used to calculate the lattice temperature. In the present case only the (111) reflection have been presented, as it is by far the strongest peak. Consequently, we discuss only the thermal expansion in the $\langle 111 \rangle$ direction and melting as a loss of the long-range order in that particular direction. At least as long as the elastic excitation in the lower power level is concerned (see following chapter) the analysis of the (200) reflection gives identical results. We have no indication that crystal anisotropy should be of importance in the present case.

III. PARTICLE COOLING

Figure 2 displays the relative lattice parameter change $\Delta a/a$ as function of delay τ between laser and x-ray pulses. At a laser power of 14.7 mW a maximum expansion of 0.91% is observed. The rise time of the signal is essentially determined by the full width at half maximum (FWHM) pulse width of the x rays of 90 ps. After the initial expansion a relaxation of the lattice parameter is observed, indicating the cooling of the particle by the surrounding liquid. In addition, within the first 100 ps strong distortions of the Lorentzian peak shapes are present, which indicate strong strain in

the particles. This is consistent with coherent lattice vibrations typically observed in time-resolved optical pump-probe experiments. The strain-induced peak broadening decays within 350 ps.

For comparison with the experiment, we perform model calculations of the particle cooling. Similarly to Wilson *et al.*,[22] we assume in our calculations a finite thermal interface conductance and a negligible temperature gradient within the particle. The excitation conditions present in our case make it possible to operate in the Laplace domain. The heat transfer equations for a spherical particle in an ambient medium with diffusive heat transport are given by

$$Mc_p \cdot (s \cdot T_p(s) - T_0) + 4\pi R^2 G \cdot (T_p(s) - T_f(r=R,s)) = 0 \tag{1}$$

$$\left. \frac{\partial}{\partial r} T_f(r,s) \right|_{r=R} + G/K \cdot (T_p(s) - T_f(r,s)) = 0, \tag{2}$$

where s denotes the time-conjugated variable in the Laplace domain. T_0 is the initial temperature of the nanoparticle with radius R, mass M, and specific heat c_p. $T_f(r,t)$ is the temperature of the surrounding fluid with thermal conductivity K, density ρ, and specific heat c. G is the interface conductance. The temperature T_p of the particle at time t after the excitation is obtained by inverse Laplace transformation as[38]

$$T_p(t) = \frac{2kR^2g^2T_0}{\pi} \int_0^\infty \frac{\exp(-\kappa u^2 t/R^2)u^2 du}{(u^2(1+Rg) - kRg)^2 + (u^3 - kRgu)^2}, \tag{3}$$

where the diffusivity $\kappa = K/(\rho c)$ is introduced. The abbreviations $k = 4\pi R^3 \rho c/(Mc_p)$ and $g = G/K$ are used for the sake of compactness. The integral is solved numerically using material constants for gold and water from the literature.[39,40] Calculating $\Delta a/a(t)$ from $T_p(t)$, we fit the decay of the lattice expansion using G as a fit parameter. The best estimate for the conductance is $G = (105 \pm 15)$ MW/(m² K). This result is close to the value $G = 130$ MW/(m² K) reported for platinum nanoparticles in water.[22]

A special case is present if heat conduction is much faster in the ambient medium than across the interface between the heat source and the medium. Then the temperature of the water layer at the particle-water interface may be expected to remain nearly constant throughout the particle cooling. The particle temperature then decays exponentially according to[41]

$$T_p(t) - T_0 = (T_p(t) - T_0)_{\max} \cdot \exp\left[-t \cdot \left(\frac{\rho_p c_p R}{3G}\right)^{-1}\right], \tag{4}$$

where ρ_p is the density of gold. In this approach the relaxation time, i.e., cooling time, will depend linearly on the particle radius R. A linear relation has indeed been observed in glass-embedded silver nanoparticles, and an interface conductance of $G = (190 \pm 15)$ MW/(m² K) has been determined.[23] In the present case of gold nanoparticles in water, however, K is lower than for silver nanoparticles in glass. Therefore the temperature rise of the water layer adjacent to the particle cannot be neglected. This leads to a reduced cooling, in particular at long time delays, and to a

nonexponential temperature decay. Thus the full solution, Eq. (3), to the heat transfer equations has to be used.

Another special case has been treated by Inouye *et al.*,[21] Hu and Hartland,[26] and Seifert, Patzlaff, and Graener.[27] This situation occurs if the heat conduction is much slower in the ambient medium than across the interface. Formally this case corresponds to $G/K \to \infty$. The solution to the heat transfer equations is given by a nonexponential decay of the particle temperature. Hu and Hartland[26] have approximated the decay by a stretched exponential with stretching parameter γ

$$T_p(t) - T_0 = (T_p(t) - T_0)_{\max} \cdot \exp(-(t/\tau)^\gamma). \quad (5)$$

They have derived values of γ around 0.7 from a comparison with the experiment. The decay times vary systematically with the size of the spheres as

$$\tau \propto R^n, \quad (6)$$

where $n = 2$. We note that when we do the same approximation and fit stretched exponential decays to the full solution [Eq. (3)] as in Fig. 2, we obtain an exponent of $n = 1.46$, which lies between the two extreme cases of particle cooling limited by thermal interface resistance and by the thermal resistivity of the ambient medium. Our results thus show that the finite thermal interface resistance is an important effect controlling the cooling of metal nanoparticles in a condensed matrix.

IV. NANOPARTICLE MELTING

Hartland, Hu, and Sader[16] have attempted to pinpoint the melting transition via the elastic properties of the nanoparticles. They measured the vibration frequency of the breathing mode with high precision but have found no discontinuity at the melting point. They conclude that a saturation of light absorption limits the energy that can be transferred to the lattice. They raised the temperature nominally to values which were up to two times higher than the melting point of gold at 1065 °C. The lattice expansion may serve as a more direct way to monitor the particle temperature as well as the melting transition.

For the determination of the melting transition the laser excitation power is raised step-wise while monitoring the Bragg peak of the particles at a delay time of $\tau = 105$ ps. The lattice expansion in the solid phase is derived from the Bragg peak position. In Fig. 3(a) the lattice expansion is plotted against the time-averaged power of the femtosecond laser. $\Delta a/a$ increases approximately linearly with increasing laser power, up to a power of 15 mW. At larger excitation levels the expansion flattens while the peak intensity decreases [see Fig. 3(b)].

For comparison, we have calculated the expansion expected from the experimental conditions, using no adjustable parameters. In particular, we have taken into account the laser repetition rate of 896 Hz, the focus size of 0.33 mm FWHM,[42] and bulk thermodynamic parameters of gold, similarly to Ref. 16. We note that for particle sizes above 10 nm the thermal expansion coefficient and heat capacity (see Table I) are not expected to deviate significantly from the bulk case at temperatures below the onset of surface
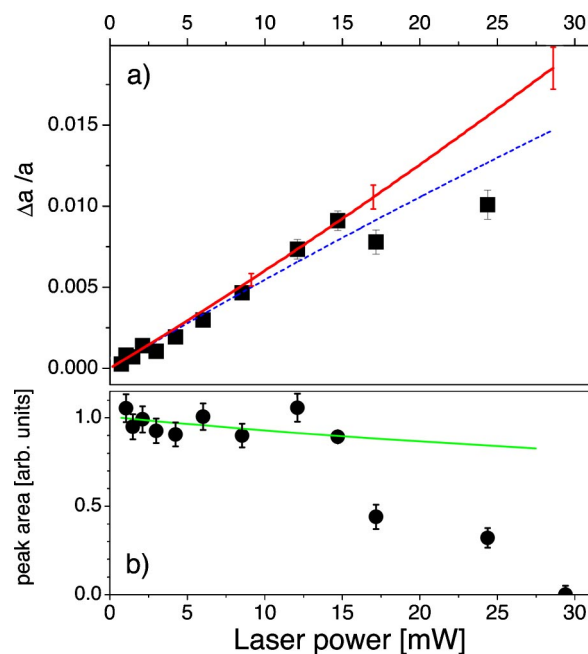

FIG. 3. (Color online) (a) Relative lattice expansion at a fixed delay of 105 ps as a function of incident laser power. The solid line is the result of a calculation of the expected expansion, when bulk constants of gold and details of the experimental setup as listed in Table I are considered. The line ends where lattice melting should occur for the bulk. The dashed line for comparison represents a constant expansion coefficient of 0.000 0142 K^{-1}. (b) Scattering intensities of the (111) reflection as function of laser excitation power (dots). The solid line shows the calculated Debye-Waller reduction of the scattering intensity at increasing lattice temperature (see Ref. 48).

melting.[43] We have checked this expectation by measuring the thermal expansion coefficient of 60 nm gold nanoparticles in a separate static experiment on particles supported on a surface. For particles the thermal expansion coefficient is $14.4(2) \times 10^{-6}$ K^{-1} at room temperature, which is the same as in the bulk within our confidence interval. At higher temperatures the values from Ref. 44 are used.

As shown in Fig. 3(a), the experimental and calculated expansion are in good agreement at low excitation powers. This implies linear absorption of light and complete transformation of the absorbed energy into lattice heat. Above 15 mW, however, the measured expansion strongly deviates from the calculated one. This deviation cannot be explained by bleaching of the interband absorption due to depletion of the 5d band,[26] since in our experiments on the average less than 0.1 d electrons per gold atom are excited into the 6sp-band; moreover, these d electrons will be replaced via fast Coulomb scattering in a few tens of femtoseconds, i.e., within less than the pulse duration.[45]

Figure 3(a) shows a gradual decrease of the scattering intensity up to a time-averaged laser power of 15 mW. This drop can be explained by the scattering reduction according to the Debye-Waller factor as calculated for bulk gold [solid line in Fig. 3(a)]. At powers above 15 mW, the peak vanishes quickly, which indicates that melting sets in. When melting occurs, the absorbed energy should partially be incorporated

TABLE I. Parameters used for calculating the nominal particle expansion as function of laser power.

	Values	Reference
Laser repetition rate	896 Hz	
Laser focus (FWHM)	0.334 mm	Knife edge scan
Capillary diameter	0.3 mm	
X-ray beam size	0.08×0.1 mm^2	
Slab extinction at 400 nm	0.077	
Mie scattering loss	37%	Mie calculation[1]
Atomic gold concentration	0.93 mol/l	
Heat capacity (constant)	23.81 J/(K mol)	16,39
Heat capacity (first temperature derivative)	0.005 J/(K mol)	16,39
Linear expansion coefficient ($\times 10^6$)		(after 44 valid in between 300 and 1300 K)
Constant	12.002 69	
First derivative	0.009 53	
Second derivative	$-8.40E\text{-}06$	
Third derivative	$5.43E\text{-}09$	
Heat of fusion	12.4 kJ/mol	16,39

as heat of fusion, thus reducing the expansion of the crystalline core with respect to the nonmelting case. This explains the deviation of the measured expansion from the calculated one above 15 mW in Fig. 3(a). It is, however, remarkable that this melting transition occurs so far below the bulk melting temperature of 1336 K (which would correspond to a laser power of approximately 28 mW in our experiment). Indeed our experiments have never shown any lattice expansion above about 1.2%, whereas an expansion of 1.82% is expected at the bulk melting temperature. The reduction of the melting temperature with size is a well known effect.[43] For instance, 8 nm sized platinum nanoparticles have recently been shown to suffer a melting point depression from a bulk value of 1770 to 600 °C.[46] However, the melting point depression is usually important only for particles below 10 nm in diameter, which is not the case in the present study, even if the grains within one particle are taken as reference. On the other hand, the effects of surface melting are important for all particles sizes. Calculations on lead particles[47] show that surface melting should occur at temperatures as low as 70% of the melting point. We expect that a liquid layer exists around a crystalline core in the power range where the scattering intensity is reduced. Unfortunately, our peak profiles do not allow us to prove that melting in our gold nanoparticles starts from the surface, as the peak width and particles size are essentially decoupled due to the polycrystalline nature of the particles.

Figure 4 displays the scattering profiles for various delay times and excitation powers. At a time-averaged power of 14.7 mW we observe a maximum $\Delta a/a$ of 0.91% corresponding to a nominal lattice temperature increase of 529 K. The peak shift to lower angles relaxes back on a nanosecond time scale and finally returns to zero when approaching complete thermal equilibrium. After a delay of 1 μs the peak shape is completely restored, demonstrating that the particles are not damaged by the laser excitation, and that the crystallite size did not change. We conclude that no melting has

occurred up to this point. The situation changes completely when the laser power is doubled. When calculating the nominal particle temperature from the energy absorbed per unit cell and the heat of fusion, this power level should be sufficient to reach the two-phase region, where solid and liquid gold coexist (almost half of the volume should be molten). In fact we see that the Bragg peak disappears, which indicates that the long-range order has completely vanished at a time delay of 100 ps. As far as the experimental resolution, which is limited by the counting statistics, allows us to assert, no crystalline material remains. This melting process must be faster than 100 ps, which is the time resolution of the experiment. After 5 ns the peak partially reappears, indicating that recrystallization starts after times much longer than the cooling times observed in the previous section. This is an indication of a slow nucleation rate of solidification. The late recrystallization could also be caused by a change of the local solvent environment, which is strongly heated and could form a gas layer at the metal surface; this could then lead to longer cooling times than at the low excitation powers studied in the previous section. However, the position of the peak at 5 ns is not where it would be expected for solid gold at the bulk melting point, but is already quite close to the reference without laser excitation. This observation favors an explanation in terms of slow nucleation. Finally, at 1 μs the peak is restored with the same width. This fact would imply that the particles are completely intact after solidification and the transition is reversible. However, two effects could counterbalance each other. First, the particles may be reduced in size or disappear due to fragmentation, which would broaden the peak or reduce the scattering intensity. At the same time the resolidified particles could be of better crystalline quality, which in turn enhances the intensity and sharpens the scattering profiles. Raising the power beyond 29 mW leads to reduced scattering at a delay time of 1 μs, pointing towards severe fragmentation processes. The importance of fragmentation is a point that clearly deserves further studies.
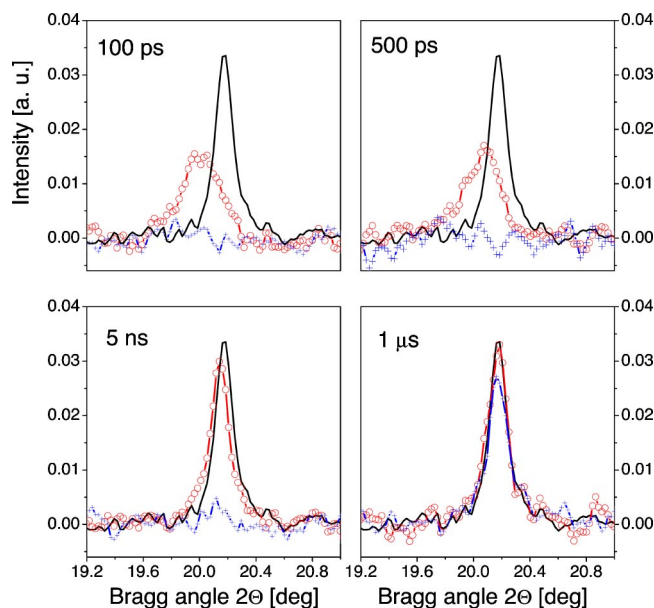
FIG. 4. (Color online) Peak profiles of the (111) reflection at different delay times and excitation powers. The black solid line in each case is the peak as observed without laser excitation, reflecting the static structure of the particles. The open circles correspond to a laser power of 14.7 mW, equivalent to 529 K lattice heating. For the crosses the laser energy is doubled to 29 mW, thus the temperature approaches the bulk melting point.

V. CONCLUSION

Time-resolved x-ray scattering has been used to directly resolve lattice changes in gold nanoparticles in water, which have been subjected to intense laser pulses. The pulses heat the particles by several hundreds of Kelvin. While the rise of the lattice temperature is too fast to be resolved in our experiment, which has a 100 ps time resolution, we were able to follow the cooling of the lattice, which transfers its energy to the surrounding water matrix. Bragg scattering additionally reveals transient strain that is present in the particles during the first hundred picoseconds, pointing to coherent particle vibrations. In contrast to the findings in Ref. 26 we have no indications that the heat transfer to the surrounding should be governed solely by the heat conductivity of the water matrix, but the temperature decay is consistent with a finite heat transfer through the interface. A value of (105 ± 15) MW/(m^2 K) is deduced for the thermal interface conductance. At high laser pulse energies the behavior is no longer elastic and power-dependent studies show that structural disorder effects already occur below the bulk melting point. When increasing the intensity further a complete disordering of the atomic arrangement is observed, which proves that a melting transition takes place. This melting transition occurs within the first 100 ps after excitation. Recrystallization occurs after large time delays; this could be a consequence of either slow solidification or slow cooling due to an insulating gas layer forming around the hot particles. Possibly the complicated behavior of the particle lattice just below the bulk melting point, where we observe partial dis-

order, could be the reason for the absence of a sharp discontinuity in the works of Hartland, Hu, and Sader[16] who could not identify the melting transition by optical methods.

It would be desirable to further investigate the melting transition in metal nanoparticles excited by short laser pulses. One would have to differentiate between partial melting of the particle ensemble and that of the structure of each single particle. With a better size dispersion an independent structural information could be obtained via small angle scattering, which can resolve the radial density distribution within the particles. Time-resolved scattering setups are fully applicable for this technique. Furthermore, the demands in momentum resolution are by far lower than for Bragg scattering; this would open up the way for applying advanced x-ray bandwidth schemes[49] in order to increase the signal-to-noise ratio.

Finally, the experiment presented here has a time resolution that is limited by the natural pulse lengths of electron bunches in a circular accelerator machine. These pulse lengths are tightly connected to the operation parameters of the machine. There are already alternative solutions available to increase the time resolution towards the 1 ps range by pulse slicing, streak cameras[50] or even new accelerators.

*Author to whom correspondence should be addressed. Electronic address: anton.plech@uni-konstanz.de

[1] U. Kreibig and M. Vollmer, *Optical Properties of Metal Clusters* (Springer, Berlin, 1995).

[2] J. R. Krenn, A. Leitner, and F. R. Aussenegg, Metal Nano-Optics, in *Encyclopedia of Nanoscience and Nanotechnology*, edited by H. S. Nalwa (American Scientific, Stevenson Ranch, CA, 2003).

[3] C. Sönnichsen, T. Franzl, T. Wilk, G. von Plessen, and J. Feldmann, New J. Phys. **4**, 93.1 (2002).

[4] S. Link and M. A. El-Sayed, Int. Rev. Phys. Chem. **19**, 409 (2000), and references therein.

[5] M. Perner, P. Bost, U. Lemmer, G. von Plessen, J. Feldmann, U. Becker, M. Mennig, M. Schmitt, and H. Schmidt, Phys. Rev. Lett. **78**, 2192 (1997).

[6] J. Hodak, I. Martini, and G. V. Hartland, Chem. Phys. Lett. **284**, 135 (1998).

[7] N. Del Fatti and F. Vallee, Appl. Phys. B: Lasers Opt. **73**, 383 (2001).

[8] T. D. Krauss and F. W. Wise, Phys. Rev. Lett. **79**, 5102 (1997).

[9] M. Nisoli, S. De Silvestri, A. Cavalleri, A. M. Malvezzi, A. Stella, G. Lanzani, P. Cheyssac, and R. Kofman, Phys. Rev. B **55**, R13 424 (1997).

[10] J. H. Hodak, A. Henglein, and G. V. Hartland, J. Chem. Phys. **111**, 8613 (1999).

[11] G. Cerullo, S. De Silvestri, and U. Banin, Phys. Rev. B **60**, 1928 (1999).

[12] M. Perner, S. Grésillon, J. März, G. von Plessen, J. Feldmann, J. Porstendorfer, K.-J. Berg, and G. Berg, Phys. Rev. Lett. **85**, 792 (2000).

[13] N. Del Fatti, C. Voisin, F. Chevy, F. Vallée, and C. Flytzanis, J. Chem. Phys. **110**, 11 484 (1999); C. Voisin, N. del Fatti, D. Christofilos, and F. Vallée, J. Phys. Chem. **105**, 2264 (2001).

[14] G. V. Hartland, M. Hu, O. Wilson, P. Mulvaney, and J. E. Sader, J. Phys. Chem. B **106**, 743 (2002).

[15] G. V. Hartland, J. Chem. Phys. **116**, 8048 (2002).

[16] G. V. Hartland, M. Hu, and J. E. Sader, J. Phys. Chem. B **107**, 7472 (2003).

[17] W. Qian, H. Yan, J. J. Wang, Y. H. Zoua, L. Lin, and J. L. Wu, Appl. Phys. Lett. **74**, 29 (1999).

[18] P. Verma, W. Cordts, G. Irmer, and J. Monecke, Phys. Rev. B **60**, 5778 (1999).

[19] B. Palpant, H. Portales, L. Saviot, J. Lermé, B. Prével, M. Pellarin, E. Duval, A. Perez, and M. Broyer, Phys. Rev. B **60**, 17 107 (1999); H. Portales, L. Saviot, E. Duval, M. Fuji, S. Hayashi, N. del Fatti, and F. Valleé, J. Chem. Phys. **115**, 3444 (2001); A. Courty, I. Lisiecki, and M. P. Pileni, *ibid.* **116**, 8074 (2002).

[20] M. H. Kuok, H. S. Lim, S. C. Ng, N. N. Liu, and Z. K. Wang, Phys. Rev. Lett. **90**, 255502 (2003).

[21] H. Inouye, K. Tanaka, I. Tanahashi, and K. Hirao, Phys. Rev. B **57**, 11 334 (1998).

[22] O. M. Wilson, X. Hu, D. G. Cahill, and P. V. Braun, Phys. Rev. B **66**, 224301 (2002).

[23] A. Plech, M. Wulff, S. Kuerbitz, K.-J. Berg, G. Berg, H. Graener, S. Grésillon, M. Kaempfe, J. Feldmann, and G. von Plessen, Europhys. Lett. **61**, 762 (2003).

[24] A. Plech, S. Grésillon, G. von Plessen, K. Scheidt, and G. Naylor,

[25] F. Cooper, Int. J. Heat Mass Transfer **20**, 991 (1977).

[26] M. Hu and G. V. Hartland, J. Phys. Chem. B **106**, 7029 (2002).

[27] G. Seifert, T. Patzlaff, and H. Graener, Phys. Rev. Lett. **88**, 147402 (2002).

[28] S. Link and M. A. El-Sayed, J. Chem. Phys. **114**, 2362 (2001).

[29] K. Sokolowski-Tinten, Ch. Blome, C. Dietrich, A. Tarasevitch, M. Horn von Hoegen, D. von der Linde, A. Cavalleri, J. A. Squier, and M. Kammler, Phys. Rev. Lett. **87**, 225701 (2001).

[30] A. Cavalleri, Cs. Tóth, C. W. Siders, J. A. Squier, F. Ráksi, P. Forget, and J. C. Kieffer, Phys. Rev. Lett. **87**, 237401 (2001).

[31] J. Turkevich, P. C. Stevenson, and J. Hillier, Discuss. Faraday Soc. **11**, 55 (1951); B. V. Enüstün and J. Turkevich, J. Am. Chem. Soc. **85**, 3317 (1963).

[32] Sizes of the particles are determined by the interplay of nucleation and growth of aggregates, therefore sizes and size distributions are as well sensitive on the solution temperature.

[33] J. Schmitt, P. Mächtle, D. Eck, H. Möhwald, and C. A. Helm, Langmuir **15**, 3256 (1999), and supporting information.

[34] A. Plech and T. Salditt, in *Handbook of Polyelectrolytes and Their Applications*, edited by H. S. Nalwa and S. Tripathy (American Scientific, Stevenson Ranch, CA, 2002).

[35] B. E. Warren, *X-ray Diffraction reprint* (Dover, New York, 1990)

[36] F. Schotte, S. Techert, P. A. Anfinrud, V. Srajer, K. Moffat, and M. Wulff, in *Third-Generation Hard X-ray Synchrotron Radiation Sources*, edited by D. Mills (Wiley, New York, 2002).

[37] M. Wulff, A. Plech, L. Eybert, R. Randler, F. Schotte, and P. Anfinrud, Faraday Discuss. **122**, 13 (2003).

[38] H. S. Carslaw and J. C. Jaeger, *Conduction of Heat in Solids* (Oxford University Press, Oxford, 1959).

[39] *American Institute of Physics Handbook*, 3rd ed., edited by Dwight E. Gray (McGraw-Hill, New York, 1972).

[40] *CRC Handbook of Chemistry and Physics*, 82nd ed. (CRC, Boca Raton, FL, 2001).

[41] A. Bejan, *Heat Transfer* (Wiley, New York, 1993).

[42] The laser spot size has been determined by measuring the laser intensity at the sample position as function of the position of a sharp blade shadowing a part of it. The laser spot was taken to be round with a Gaussian intensity distribution. The x-ray illuminated volume accounts for only a fraction of it in the spot center.

[43] P. Buffat and J. P. Borel, Phys. Rev. A **13**, 2287 (1976).

[44] Y. S. Touloukian, R. K. Kirby, R. E. Taylor, and P. D. Desai, Thermal expansion — Metallic elements and alloys, in *Thermodynamical Properties of Matter* (IFI Plenum, New York, 1975), Vol. 12.

[45] V. P. Zhukov, F. Aryasetiawan, E. V. Chulkov, I. G. de Gurtubay, and P. M. Echenique, Phys. Rev. B **64**, 195122 (2001).

[46] Z. L. Wang, J. M. Petroski, T. C. Green, and M. A. El-Sayed, J. Phys. Chem. B **102**, 6145 (1998).

[47] H. Sakai, Surf. Sci. **351**, 285 (1996).

[48] J. M. Ziman, *Principles of the Theory of Solids*, 2nd ed. (Cambridge University Press, London, 1972).

[49] A. Plech, R. Randler, A. Geis, and M. Wulff, J. Synchrotron Radiat. **9**, 287 (2002).

[50] G. A. Naylor, K. Scheidt, J. Larsson, M. Wulff, and J. M. Filhol, Meas. Sci. Technol. **12**, 1858 (2001).

Chem. Phys. **298**, 55 (2004).